

Comparison of nonlinear field-split preconditioners for two-phase flow in heterogeneous porous media

Mamadou N'diaye^{a,*}, François P. Hamon^b, Hamdi A. Tchelepi^a

^a*Energy Resources Engineering, Stanford University, Stanford, United States*

^b*TotalEnergies E&P Research & Technology USA, LLC, United States*

Abstract

This work focuses on the development of a two-step field-split nonlinear preconditioner to accelerate the convergence of two-phase flow and transport in heterogeneous porous media. We propose a field-split algorithm named Field-Split Multiplicative Schwarz Newton (FSMSN), consisting in two steps: first, we apply a preconditioning step to update pressure and saturations nonlinearly by solving approximately two subproblems in a sequential fashion; then, we apply a global step relying on a Newton update obtained by linearizing the system at the preconditioned state. Using challenging test cases, FSMSN is compared to an existing field-split preconditioner, Multiplicative Schwarz Preconditioned for Inexact Newton (MSPIN), and to standard solution strategies such as the Sequential Fully Implicit (SFI) method or the Fully Implicit Method (FIM). The comparison highlights the impact of the upwinding scheme in the algorithmic performance of the preconditioners and the importance of the dynamic adaptation of the subproblem tolerance in the preconditioning step. Our results demonstrate that the two-step nonlinear preconditioning approach—and in particular, FSMSN—results in a faster outer-loop convergence than with the SFI and FIM methods. The impact of the preconditioners on computational performance—i.e., measured by wall-clock time—will be studied in a subsequent publication.

Keywords: Nonlinear solver, field-split preconditioning methods, two-phase flow, coupled multi-physics problems

1. Introduction

The numerical simulation of multiphase flow and transport in geological porous media requires solving complex partial differential equations (PDEs) with highly nonlinear saturation-dependent coefficients [1, 2]. In most subsurface applications, the heterogeneity of the porous medium generates large spatial variations in the flow regimes with high velocities near the wells and in high-permeability regions. This leads to severe stability constraints on the time step size in explicit discretization schemes. Therefore, unconditionally stable implicit schemes are often the temporal discretization method of choice for porous media flow problems.

However, solving the nonlinear systems resulting from an implicit discretization of the PDEs is challenging and often represents most of the computational cost of the simulations. In the Fully Implicit Method (FIM), all the degrees of freedom of the system—typically, pressure, saturations, and compositions—are updated simultaneously using Newton's method with damping [3]. This requires solving large, ill-conditioned linear systems at each nonlinear iteration which is computationally expensive. In addition, for highly nonlinear problems and/or large time steps, Newton's method often fails to converge, in which case the time step is restarted from the previous converged state with a reduced size. To avoid these convergence failures, globalization methods have been developed to enlarge the convergence radius of Newton's method. Popular damping methods for the Newton updates include saturation chopping based on heuristics [4] or relying on the structure of the fractional flow function [5–8]. In the Sequential Fully Implicit (SFI) method [9–13], the system is decomposed into two subproblems—namely, flow and transport—to

*Corresponding author.

Email addresses: mndiaye@uphf.fr/ndiaye.mamadou24@gmail.com (Mamadou N'diaye), francois.hamon@totalenergies.com (François P. Hamon), tchelepi@stanford.edu (Hamdi A. Tchelepi)

avoid solving large coupled linear systems involving all the degrees of freedom. In this approach, the subproblems are solved sequentially using specialized nonlinear solvers until convergence of the outer loop is attained. However, this decoupled approach often suffers from slow outer loop convergence for tightly coupled physics (e.g., in the presence of strong buoyancy and capillary effects) and may require the use of dedicated convergence accelerators for challenging problems [14–17].

In recent years, advanced nonlinear strategies have been proposed to overcome the limitations of Newton-based FIM and of SFI for multiphase flow in porous media. Although a comprehensive review is out of the scope of the present work, we mention some of the recently presented nonlinear solution strategies. They include homotopy methods [3, 18, 19], in which a sequence of prediction-correction steps is used to follow a suitably parameterized homotopy path leading to the solution. Homotopy methods are robust for large time steps and can achieve, in some cases, unconditional nonlinear convergence. Using a different approach, ordering-based methods [20–24] accelerate nonlinear convergence thanks to a reordering technique based on the flow direction. The reordered systems have block-triangular structure and can therefore be efficiently solved with backward substitution. To obtain highly scalable solvers able to take large time steps, multilevel solution algorithms relying on the application of the multigrid principles at the nonlinear level in a Full Approximation Scheme (FAS) have been proposed [25–28].

The efforts to design efficient nonlinear preconditioners to the Newton update are particularly relevant to this work. Two distinct directions have been explored. A class of nonlinear preconditioners leverages domain decomposition methods [29–33] to precondition the nonlinear system in a computationally inexpensive way and speed up convergence. In this work, we focus on nonlinear preconditioners obtained by splitting the system by physical field [34–36]. Instead of decomposing the domain in space, field-split preconditioners exploit the mathematical structure of the nonlinear system to split the problem into multiple subproblems solved nonlinearly at a loose tolerance before the computation of a global update for all the degrees of freedom. This approach provides an efficient framework to precondition the system field by field to compute more accurate nonlinear updates and in turn, accelerate nonlinear convergence [37, 38]. In the context of mixed elliptic-hyperbolic multiphase flow and transport in porous media, the method is particularly attractive since it retains the best features of both SFI and FIM. Specifically, the preconditioning step resembles the SFI outer iteration based on a pressure update followed by a saturation update and therefore does not involve solving a large coupled linear system. The global step of field-split algorithms plays the role of the computation of the Newton update in FIM and maintains robust convergence properties for strongly coupled problems.

In this work, we focus on immiscible two-phase flow in porous media and compare various field-split preconditioners based on the pressure-saturation decomposition. We consider the Multiplicative Schwarz Preconditioned for Inexact Newton (MSPIN) proposed in [39], in which the solution of the preconditioning step is used to compute an approximation of the preconditioned Jacobian system. The global step consists in solving this global preconditioned system to obtain the updated pressures and saturations. We also propose an alternative method, Field-Split Multiplicative Schwarz Newton (FSMSN) in which the preconditioning step is the same as in MSPIN, but the global step is simply the Newton update computed by linearizing the system at the preconditioned state. We compare MSPIN and FSMSN to SFI and Newton with damping for FIM on challenging two-phase flow test cases. The comparison takes into account the role of the upwinding scheme—Phase Potential Upwinding [40, 41] or Implicit Hybrid Upwinding [11, 42–48]—as well as the role of the nonlinear tolerance used in the subproblems. To do so, we propose an adaptive method to compute the subproblem nonlinear tolerance at each preconditioning step, as typically done in inexact Newton methods [49–54]. We demonstrate that the two-step nonlinear preconditioners and, in particular, FSMSN, are successful at accelerating nonlinear convergence and are worth being explored as viable options to reduce the computational cost of reservoir simulation—which will be addressed in a future publication.

The structure of the present article is as follows. We review the PDEs governing two-phase flow and transport in porous media in Section 2. The fully implicit finite-volume scheme is reviewed in Section 3. The two nonlinear preconditioning techniques considered here—namely, FSMSN and MSPIN—are reviewed in Sections 4 and 5, respectively. The method used to compute the adaptive subproblem tolerance is presented in Section 6. We compare the efficiency of the nonlinear preconditioners with numerical examples in Section 7.

2. Governing equations

Let $\bar{\Omega} = \Omega \cup \Gamma$ be a closed set in \mathbb{R}^2 , with Ω an open set and Γ its boundary. We note $\mathbb{I} = [0, t_{max}]$ a finite time interval with $t_{max} > 0$ the maximal time. We denote the spatial coordinates by $\mathbf{x} \in \Omega$ and the time coordinate by $t \in \mathbb{I}$.

We consider the immiscible flow of two fluid phases in an incompressible porous medium, with a wetting (w) and a non-wetting (nw) phase. For a phase $\ell \in \{nw, w\}$, the mass conservation equation reads

$$\phi \frac{\partial(\rho_\ell s_\ell)}{\partial t} - \nabla \cdot (\rho_\ell \mathbf{u}_\ell(p, s)) = q_\ell, \quad \ell \in \{nw, w\}, \quad \text{on } \Omega \times \mathbb{I}, \quad (1)$$

where $\phi = \phi(\mathbf{x})$ is the porosity of the medium, $q_\ell = q_\ell(\mathbf{x})$ is the source/sink term with the convention that $q_\ell > 0$ for injection, and $q_\ell < 0$ for production. The saturation $s_\ell = s_\ell(\mathbf{x}, t)$ represents the fraction of the pore volume occupied by phase ℓ , with the following constraint:

$$\sum_\ell s_\ell = 1. \quad (2)$$

We choose the wetting-phase saturation as the primary saturation unknown, denoted by $s := s_w$. Using the saturation constraint (2), we write all the saturation-dependent properties as a function of s only. The phase velocity \mathbf{u}_ℓ of a phase ℓ is given by Darcy's law

$$\mathbf{u}_\ell(p, s) = -k\lambda_\ell(\nabla p - \rho_\ell g \nabla d), \quad \ell \in \{nw, w\}, \quad (3)$$

where we have neglected capillary pressure. In (3), $p(\mathbf{x}, t)$ is the pressure, $k(\mathbf{x})$ is the scalar rock permeability, ρ_ℓ is the phase density, and $\lambda_\ell(s) = k_{r\ell}(s)/\mu_\ell$ is the phase mobility, defined as the phase relative permeability, $k_{r\ell}(s)$, divided by the phase viscosity μ_ℓ . The gravitational acceleration is g and the depth is d (positive going downward). Inserting the expression of the phase velocity given by Darcy's law (3) into the mass conservation equation (1) gives rise to the following form of the two-phase flow and transport equation:

$$\phi \frac{\partial(\rho_\ell s_\ell)}{\partial t} - \nabla \cdot (k\lambda_\ell(\nabla p - \rho_\ell g \nabla d)) = q_\ell, \quad \ell \in \{nw, w\}, \quad \text{on } \Omega \times \mathbb{I}. \quad (4)$$

In the sequential and field-split solution methods considered in this work, we employ a discretization scheme applied to a split form of the governing equations consisting of an elliptic pressure equation coupled with a hyperbolic transport problem. The pressure subproblem is obtained by summing the mass balance equations (4) over the two phases. Using the saturation constraint (2) and assuming that the two phases are incompressible, we obtain

$$\nabla \cdot \mathbf{u}_T(p, s) = \sum_\ell q_\ell, \quad (5)$$

where the total velocity \mathbf{u}_T is defined by $\mathbf{u}_T(p, s) := \sum_\ell \mathbf{u}_\ell(p, s)$. The transport problem is obtained by eliminating the pressure variable in the flux term of (4) to obtain the following fractional flow formulation:

$$\phi \frac{\partial(\rho_\ell s_\ell)}{\partial t} + \nabla \cdot \left(\frac{\lambda_\ell}{\lambda_T} \mathbf{u}_T(p, s) + k \frac{\lambda_m \lambda_\ell}{\lambda_T} (\rho_\ell - \rho_m) g \nabla d \right) = q_\ell, \quad m, \ell \in \{nw, w\}, m \neq \ell, \quad (6)$$

where $\lambda_T(s) := \sum_\ell \lambda_\ell(s)$ is the total mobility.

3. Discretization scheme

Given a mesh consisting of M cells, we use first-order finite-volume scheme. We consider $0 = t^0 \leq t^1 \leq \dots \leq t^N = t_{max}$, $N \in \mathbb{N}$ a finite discretization of the temporal axis, and $\Delta t^{n+1} := t^{n+1} - t^n$, $0 \leq n \leq N$, $n \in \mathbb{N}$ the time step. We use a (backward-Euler) fully implicit scheme for the integration in time. We denote by $\mathbf{p}^{n+1} := [p_1^{n+1}, \dots, p_M^{n+1}]^\top$ and $\mathbf{s}^{n+1} := [s_1^{n+1}, \dots, s_M^{n+1}]^\top$, the solution pair $(\mathbf{p}^{n+1}, \mathbf{s}^{n+1})$ the vectors collecting respectively the pressure and saturation unknowns. To define the discrete problem, we first introduce the phase-based residual in cell K at time $n+1$, $r_{\ell,K}^{n+1}$, as

$$r_{\ell,K}^{n+1}(\mathbf{p}^{n+1}, \mathbf{s}^{n+1}) := V_K \phi_K \frac{\rho_{\ell,K}^{n+1} s_{\ell,K}^{n+1} - \rho_{\ell,K}^n s_{\ell,K}^n}{\Delta t^{n+1}} + \sum_{L \in \text{adj}(K)} F_{\ell,KL}^{n+1}(\mathbf{p}^{n+1}, \mathbf{s}^{n+1}) - V_K q_{\ell,K}(p_K^{n+1}, s_K^{n+1}). \quad (7)$$

In (7), $F_{\ell,KL}^{n+1}$ is the numerical flux for the interface (KL) between cells K and L , $\text{adj}(K)$ is the set of neighbors of cell K and V_K the volume of cell K . The computation of the numerical flux is based on a Two-Point Flux Approximation

(TPFA). We consider both Phase-Potential Upwinding (PPU) [40, 41] and Implicit Hybrid Upwinding (IHU) [11, 42–47, 55] for the approximation of the transport coefficient of the flux term.

In this work, we consider two equivalent formulations of the nonlinear problem. In the Newton-based FIM, we apply the standard fully coupled Newton’s method with damping to find the solution pair $(\mathbf{p}^{n+1}, \mathbf{s}^{n+1})$ that satisfies

$$\mathbf{r}^{n+1}(\mathbf{p}^{n+1}, \mathbf{s}^{n+1}) := [\mathbf{r}_{nw}^{n+1}(\mathbf{p}^{n+1}, \mathbf{s}^{n+1}), \mathbf{r}_w^{n+1}(\mathbf{p}^{n+1}, \mathbf{s}^{n+1})]^\top = \mathbf{0}. \quad (8)$$

In sequential and field-split nonlinear solution strategies, we split the problem into a discrete pressure problem and a discrete transport problem. The solution pair $(\mathbf{p}^{n+1}, \mathbf{s}^{n+1})$ must in this case satisfy:

$$\mathbf{f}^{n+1}(\mathbf{p}^{n+1}, \mathbf{s}^{n+1}) := [\mathbf{g}^{n+1}(\mathbf{p}^{n+1}, \mathbf{s}^{n+1}), \mathbf{h}^{n+1}(\mathbf{p}^{n+1}, \mathbf{s}^{n+1})]^\top = \mathbf{0}, \quad (9)$$

where the discrete pressure problem is obtained by summing the phase-based residual equations, as in (5):

$$\mathbf{g}^{n+1}(\mathbf{p}^{n+1}, \mathbf{s}^{n+1}) := \mathbf{r}_{nw}^{n+1}(\mathbf{p}^{n+1}, \mathbf{s}^{n+1}) + \mathbf{r}_w^{n+1}(\mathbf{p}^{n+1}, \mathbf{s}^{n+1}), \quad (10)$$

and the discrete saturation problem simply consists of one of the phase-based residual equations. Here, we choose the wetting-phase residual:

$$\mathbf{h}^{n+1}(\mathbf{p}^{n+1}, \mathbf{s}^{n+1}) := \mathbf{r}_w^{n+1}(\mathbf{p}^{n+1}, \mathbf{s}^{n+1}). \quad (11)$$

From now on, we consider time step $n \in \mathbb{N}$ and describe two algorithms to compute the solution pair $(\mathbf{p}^{n+1}, \mathbf{s}^{n+1})$ of nonlinear problems (8) and (9) at time $n + 1$. For simplicity, we drop the temporal superscript denoting the time step.

4. Field-split multiplicative Schwarz Newton method

The multiplicative Schwarz method has been used to split boundary value problems (BVP) into subproblems solver on smaller physical domains [29–33]. It has also been used to split a coupled BVP into subproblems based on the physics [34–36], each subproblem being solved on the full domain to update one of the fields (here, pressure and saturation). The motivation for splitting a coupled problem according to the physics is to solve the physical subproblems one at a time (ideally, with a specialized solver) and use the individually updated fields to precondition the nonlinear iteration, yielding a faster nonlinear convergence. In this section, the objective is to use the field-split approach to construct a predictor-corrector method that converges faster than commonly used algorithms based on the Newton iteration or the sequential fully implicit iteration.

The preconditioning step of the FSMSN outer iteration consists in computing an intermediate value of the pressure and saturation, $\mathbf{p}^{k,\star}$ and $\mathbf{s}^{k,\star}$, by solving individual pressure and transport problems sequentially. We first solve nonlinearly the pressure equation. Specifically, for a fixed \mathbf{s}^k , find the update $\delta_1(\mathbf{p}^k, \mathbf{s}^k)$ such that

$$\mathbf{g}(\mathbf{p}^{k,\star}, \mathbf{s}^k) = \mathbf{0}, \quad (12)$$

where $\mathbf{p}^{k,\star} := \mathbf{p}^k + \delta_1(\mathbf{p}^k, \mathbf{s}^k)$. We solve (12) with Newton’s method to obtain a pressure prediction, $\mathbf{p}^{k,\star}$. The preconditioning step continues by solving nonlinearly a transport problem. For a fixed $\mathbf{p}^{k,\star}$, find $\delta_2(\mathbf{p}^{k,\star}, \mathbf{s}^k)$ such that

$$\mathbf{h}(\mathbf{p}^{k,\star}, \mathbf{s}^{k,\star}) = \mathbf{0}, \quad (13)$$

where $\mathbf{s}^{k,\star} := \mathbf{s}^k + \delta_2(\mathbf{p}^{k,\star}, \mathbf{s}^k)$. In (13), we explore two formulations of the discrete transport problem. In the first formulation, we use directly the intermediate pressure, $\mathbf{p}^{k,\star}$, and we consider a discrete transport equation approximating (4) for $\ell = w$. In the second formulation, we compute an intermediate total velocity field with the intermediate pressure, and we consider a discrete transport equation approximation (6) for $\ell = w$ with a fixed total velocity. This technique is commonly used in the sequential fully implicit method in which the total velocity is also fixed during the resolution of the transport problem. In both options, we use Newton’s method with damping to solve the discrete transport problem, although more efficient nonlinear solvers are available [20–24].

In the correction step, we re-evaluate the residual and Jacobian matrix with the intermediate pressure and saturation. Then, we compute the $(k + 1)$ -th solution iterate as

$$\begin{aligned} \mathbf{p}^{k+1} &\leftarrow \mathbf{p}^{k,\star} + \delta \mathbf{p}^{k+1}, \\ \mathbf{s}^{k+1} &\leftarrow \mathbf{s}^{k,\star} + \tau^{k+1} \delta \mathbf{s}^{k+1}, \end{aligned} \quad (14)$$

where τ^{k+1} is a diagonal matrix of damping parameters. In (14), the update is obtained by solving the linear system

$$\delta \mathbf{x}^{k+1} = -\mathbf{J}(\mathbf{x}^{k,*})^{-1} \mathbf{r}(\mathbf{x}^{k,*}), \quad \mathbf{x} := \begin{pmatrix} \mathbf{p} \\ \mathbf{s} \end{pmatrix}. \quad (15)$$

Note that for the assembly of \mathbf{J} in (15), the fluxes are computed using the same discretization as in the subproblems (12) and (13) to maintain a uniform discrete approach throughout the FSMSN nonlinear iteration. The implementation of FSMSN is described in Algorithm 1.

Algorithm 1 FSMSN algorithm for two-phase flow and transport

for $k = 1, \dots, k_{itermax}$ **do**
 Check convergence, and break nonlinear loop if convergence was achieved
 Pressure step:
 For a fixed \mathbf{s}^k , solve $\mathbf{g}(\mathbf{p}^{k,*}, \mathbf{s}^k) = \mathbf{0}$
 Transport step:
 For a fixed $\mathbf{p}^{k,*}$ or a fixed total velocity $\mathbf{u}_T^{k,*}$, solve $\mathbf{h}(\mathbf{p}^{k,*}, \mathbf{s}^{k,*}) = \mathbf{0}$
 Coupled step:
 Recompute residual and Jacobian using $(\mathbf{p}^{k,*}, \mathbf{s}^{k,*})$
 Solve linear system: $\delta \mathbf{x}^{k+1} = -\mathbf{J}(\mathbf{x}^{k,*})^{-1} \mathbf{r}(\mathbf{x}^{k,*})$
 Update solution: $\mathbf{p}^{k+1} \leftarrow \mathbf{p}^{k,*} + \delta \mathbf{p}^{k+1}$, $\mathbf{s}^{k+1} \leftarrow \mathbf{s}^{k,*} + \tau^{k+1} \delta \mathbf{s}^{k+1}$
end for

5. Preconditioned method based on field-split multiplicative Schwarz method

In this section, we review the construction of a preconditioned method for the two-phase problem using a field-split multiplicative Schwarz method (MSPIN). As in the previous section, the iteration consists of two steps, with first a preconditioning step following with a global step. The preconditioning step is identical to that of FSMSN. Using the same notations as in Section 4, the flow problem consists in finding a new pressure field, $\mathbf{p}^{k,*} := \mathbf{p}^k + \delta_1(\mathbf{p}^k, \mathbf{s}^k)$, that satisfies (12) for a fixed saturation field, \mathbf{s}^k . Then, the transport problem consists in finding an updated saturation field, $\mathbf{s}^{k,*} := \mathbf{s}^k + \delta_2(\mathbf{p}^k, \mathbf{s}^k)$, that satisfies (13) for a fixed pressure field, $\mathbf{p}^{k,*}$. In this second step, we only consider the formulation in which the discrete transport equation approximates (4) for $\ell = w$. The MSPIN algorithm differs from FSMSN in the global step. Once the pressure and transport problems are solved, we form the following preconditioned problem:

$$\mathcal{F}(\mathbf{p}^k, \mathbf{s}^k) := [\delta_1(\mathbf{p}^k, \mathbf{s}^k), \delta_2(\mathbf{p}^k, \mathbf{s}^k)]^\top = \mathbf{0}. \quad (16)$$

The goal of the coupled step is to form a Jacobian system from (16) and solve it to obtain the pressure and saturation updates of outer iteration k . Forming the Jacobian system requires computing the partial derivatives of δ_1 and δ_2 with respect to the pressure and saturation variables. Using the chain rule, we obtain the derivatives of δ_1 by differentiating (12), which yields:

$$\partial_p \delta_1(\mathbf{p}^k, \mathbf{s}^k) = -\mathbf{I}_M, \quad (17)$$

$$\partial_s \delta_1(\mathbf{p}^k, \mathbf{s}^k) = -(\partial_p \mathbf{g}(\mathbf{p}^{k,*}, \mathbf{s}^k))^{-1} \partial_s \mathbf{g}(\mathbf{p}^{k,*}, \mathbf{s}^k). \quad (18)$$

\mathbf{I}_M denotes a M by M identity matrix. Differentiating (13) yields the derivatives of δ_2 :

$$\partial_p \delta_2(\mathbf{p}^k, \mathbf{s}^k) = \mathbf{0}, \quad (19)$$

$$\partial_s \delta_2(\mathbf{p}^k, \mathbf{s}^k) = -\mathbf{I}_M - (\partial_s \mathbf{h}(\mathbf{p}^{k,*}, \mathbf{s}^{k,*}))^{-1} \partial_p \mathbf{h}(\mathbf{p}^{k,*}, \mathbf{s}^{k,*}) (\partial_p \mathbf{g}(\mathbf{p}^{k,*}, \mathbf{s}^k))^{-1} \partial_s \mathbf{g}(\mathbf{p}^{k,*}, \mathbf{s}^k). \quad (20)$$

Using equations (17) to (20), the Jacobian matrix, $\mathcal{J}(\mathbf{p}^k, \mathbf{s}^k)$ of (16) is then given by:

$$\mathcal{J}(\mathbf{p}^k, \mathbf{s}^k) = - \begin{pmatrix} \partial_p \mathbf{g}(\mathbf{p}^{k,*}, \mathbf{s}^k) & \mathbf{0} \\ \partial_p \mathbf{h}(\mathbf{p}^{k,*}, \mathbf{s}^{k,*}) & \partial_s \mathbf{h}(\mathbf{p}^{k,*}, \mathbf{s}^{k,*}) \end{pmatrix}^{-1} \begin{pmatrix} \partial_p \mathbf{g}(\mathbf{p}^{k,*}, \mathbf{s}^k) & \partial_s \mathbf{g}(\mathbf{p}^{k,*}, \mathbf{s}^k) \\ \partial_p \mathbf{h}(\mathbf{p}^{k,*}, \mathbf{s}^{k,*}) & \partial_s \mathbf{h}(\mathbf{p}^{k,*}, \mathbf{s}^{k,*}) \end{pmatrix} \quad (21)$$

At this point, the second matrix on the right-hand side of (21) differs from the unpreconditioned Jacobian matrix of (8) because the first row is evaluated at $(\mathbf{p}^{k,*}, \mathbf{s}^k)$, while the second row is evaluated at $(\mathbf{p}^{k,*}, \mathbf{s}^{k,*})$. Following the methodology of [39], we approximate the preconditioned Jacobian matrix of the Multiplicative Schwarz Preconditioned Inexact Newton (MSPIN) method by setting $\delta_2(\mathbf{p}^k, \mathbf{s}^k) = \mathbf{0}$ in (21), which results in:

$$\mathcal{J}(\mathbf{p}^k, \mathbf{s}^k) \approx - \begin{pmatrix} \partial_p \mathbf{g}(\mathbf{p}^{k,*}, \mathbf{s}^k) & \mathbf{0} \\ \partial_p \mathbf{h}(\mathbf{p}^{k,*}, \mathbf{s}^k) & \partial_s \mathbf{h}(\mathbf{p}^{k,*}, \mathbf{s}^k) \end{pmatrix}^{-1} \mathbf{J}(\mathbf{p}^{k,*}, \mathbf{s}^k). \quad (22)$$

where \mathbf{J} is the original, unpreconditioned Jacobian matrix of (8). We note that in (22), the two matrices on the right-hand side are now fully evaluated using the state of the system after the pressure step. Then, we obtain the $(k+1)$ -th solution iterate as

$$\begin{aligned} \mathbf{p}^{k+1} &\leftarrow \mathbf{p}^k + \delta \mathbf{p}^{k+1}, \\ \mathbf{s}^{k+1} &\leftarrow \mathbf{s}^k + \tau^{k+1} \delta \mathbf{s}^{k+1}, \end{aligned} \quad (23)$$

In (23), the update is obtained by solving the linear system:

$$\delta \mathbf{x}^{k+1} = -\mathcal{J}(\mathbf{p}^k, \mathbf{s}^k)^{-1} \mathcal{F}(\mathbf{p}^k, \mathbf{s}^k), \quad \mathbf{x} := \begin{pmatrix} \mathbf{p} \\ \mathbf{s} \end{pmatrix}. \quad (24)$$

The MSPIN iteration for two-phase flow and transport is summarized in Algorithm 2. The MSPIN strategy converges to the same solution as Newton based FIM, as proven in [39]. In [39], the authors provide numerical tests based on the Navier-Stokes equations showing that MSPIN is more robust than Newton's method and the Additive Schwarz-type preconditioning (ASPIN). In this work, we focus on the assessment of the nonlinear behavior of the MSPIN algorithm for the strongly coupled and highly nonlinear two-phase flow and transport problem. In our implementation, we form matrix (22) and solve (24) by calling a direct solver twice. In future work, we will exploit the structure of the block-triangular matrix of (22) inside an iterative Krylov-type linear solver [56, 57] to improve the efficiency of the approach on large-scale problems.

Algorithm 2 MSPIN algorithm for two-phase flow and transport

for $k = 1, \dots, k_{itermax}$ **do**

 Check convergence, and break nonlinear loop if convergence was achieved

Pressure step:

 For a fixed \mathbf{s}^k , solve $\mathbf{g}(\mathbf{p}^{k,*}, \mathbf{s}^k) = \mathbf{0}$

 Update and save $\partial_p \mathbf{g}(\mathbf{p}^{k,*}, \mathbf{s}^k)$, $\partial_s \mathbf{g}(\mathbf{p}^{k,*}, \mathbf{s}^k)$, $\partial_p \mathbf{h}(\mathbf{p}^{k,*}, \mathbf{s}^k)$, and $\partial_s \mathbf{h}(\mathbf{p}^{k,*}, \mathbf{s}^k)$

Transport step:

 For fixed $\mathbf{p}^{k,*}$, solve $\mathbf{h}(\mathbf{p}^{k,*}, \mathbf{s}^{k,*}) = \mathbf{0}$

Coupled step:

 Form preconditioned residual $\mathcal{F}(\mathbf{p}^k, \mathbf{s}^k)$ and Jacobian matrix $\mathcal{J}(\mathbf{p}^k, \mathbf{s}^k)$ as in (16) and (21)

 Solve linear system: $\delta \mathbf{x}^{k+1} = -\mathcal{J}(\mathbf{p}^k, \mathbf{s}^k)^{-1} \mathcal{F}(\mathbf{p}^k, \mathbf{s}^k)$

 Update solution: $\mathbf{p}^{k+1} \leftarrow \mathbf{p}^k + \delta \mathbf{p}^{k+1}$; $\mathbf{s}^{k+1} \leftarrow \mathbf{s}^k + \tau^{k+1} \delta \mathbf{s}^k$

end for

6. Convergence check and adaptive tolerance

In Algorithms 1 and 2, the convergence checks involved in the outer and inner loops are performed using the ℓ_2 -norm of the normalized residual. Specifically, convergence of the full problem is achieved when:

$$\max_{\ell} \left(\left\| \mathbf{diag}(\mathbf{r}_{\ell}^{k+1}(\mathbf{p}^{k+1}, \mathbf{s}^{k+1})) \mathbf{diag}(\mathbf{m}_{\ell}(\mathbf{p}^n))^{-1} \right\|_{2,2} \right) < \epsilon. \quad (25)$$

where we have used the normalizer $\mathbf{m}_{\ell}(\mathbf{p}^n) = [\rho_{\ell,1}^n V_1 \phi_1, \dots, \rho_{\ell,M}^n V_M \phi_M]^T$ evaluated at the previous converged time step, and where $\mathbf{diag}(\mathbf{x})$ is the diagonal matrix obtained from the argument vector \mathbf{x} . In the first inner loop of Algorithms 1 and 2, convergence of the pressure problem is reached when

$$\left\| \mathbf{diag}(\mathbf{g}(\mathbf{p}^{k,*}, \mathbf{s}^k)) \mathbf{diag}(\mathbf{m}_{pw}(\mathbf{p}^n) + \mathbf{m}_w(\mathbf{p}^n))^{-1} \right\|_{2,2} < \epsilon_p^k, \quad (26)$$

while, in the second inner loop, the transport problem is converged when

$$\left\| \text{diag}(\mathbf{h}(\mathbf{p}^{k,\star}, \mathbf{s}^{k,\star})) \text{diag}(\mathbf{m}_w(\mathbf{p}^n))^{-1} \right\|_{2,2} < \epsilon_s^k. \quad (27)$$

If these criteria are not satisfied, we keep iterating until we reach convergence or the maximum number of iterations. The choice of subproblem tolerances in (26) and (27) is key for the nonlinear behavior and the efficiency of the schemes. In the numerical examples, we explore the two approaches detailed below.

In the first approach, we set the subproblem tolerances, ϵ_p^k and ϵ_s^k , to constant values, ϵ_p and ϵ_s , chosen to be stricter or equal to the full problem tolerance, ϵ , used in the outer loop. This is motivated by the fact that, in MSPIN, the computation of the preconditioned Jacobian in (21) assumes that the pressure and transport subproblems are fully converged and that (12) and (13) are satisfied. However, this approach requires a significant computational effort to solve the subproblems which is likely to undermine the efficiency of the scheme.

In an alternative approach, we also explore the use of adaptive subproblem tolerances to minimize the number of subproblem iterations and reduce the computational cost of the schemes. We define the subproblem tolerances as:

$$\epsilon_p^0 = \epsilon_s^0 := 1 \quad (28)$$

$$\epsilon_p^k := \eta^k \epsilon_p^{k-1} \quad \text{and} \quad \epsilon_s^k := \eta^k \epsilon_s^{k-1}, \quad k \geq 1. \quad (29)$$

The parameter $\eta^k \in [0, 1[$ depends on the outer iteration number and is used to control the subproblem tolerance. We choose a relatively large η^k during the first outer iterations to use a relaxed tolerance, and we gradually reduce η^k to obtain a tighter tolerance as the outer loop approaches convergence. A similar approach based on the Eisenstat-Walker algorithm is commonly used to reduce the cost of solving the linear systems in the inexact Newton method (see for instance [50, 51]). Computing the parameter η^k at each outer iteration is the critical part of the algorithm. We adapt the work of [50, 51] to Algorithms 1 and 2 by setting:

$$(A_1) \quad \eta^k = 0.1, \quad k \geq 0, \quad (30)$$

$$(A_2) \quad \eta^k = 2^{-(k+1)}, \quad k \geq 0, \quad (31)$$

$$(A_3) \quad \eta^0 = 1, \quad \eta^k = \frac{\|\mathbf{r}^k(\mathbf{p}^k, \mathbf{s}^k)\|_2 - \|\mathbf{r}^{k-1}(\mathbf{p}^{k-1}, \mathbf{s}^{k-1}) + \mathbf{J}(\mathbf{x}^{k-1})\delta\mathbf{x}^{k-1}\|_2}{\|\mathbf{r}^{k-1}(\mathbf{p}^{k-1}, \mathbf{s}^{k-1})\|_2}, \quad k \geq 1. \quad (32)$$

In the next section, we refer to these approaches as A_1 , A_2 , and A_3 , respectively. The algorithm employed to compute the subproblem tolerance and use in the inner loop is illustrated in Algorithm 3 for the transport problem.

Algorithm 3 Transport inner loop with adaptive tolerance

Given $k \in \mathbb{N}^*$ the outer-loop iteration number
 Given $\epsilon_s^{k-1} \in [0, 1[$ the tolerance used at outer-loop iteration $k - 1$ ($\epsilon^0 = 1$)
 Compute η^k using (30), or (31), or (32)
 Compute the new tolerance $\epsilon_s^k = \eta^k \epsilon_s^{k-1}$
for $m = 1, \dots, m_{\text{maxiter}}$ **do**
 Compute the residual, $\mathbf{h}(\mathbf{p}^{k,\star}, \mathbf{s}^{k,m})$, and the Jacobian matrix
 if $\|\mathbf{h}(\mathbf{p}^{k,\star}, \mathbf{s}^{k,\star})/\mathbf{m}_w(\mathbf{p}^n)\|_2 < \epsilon_s^k$ **then**
 Convergence is achieved, return the solution $\mathbf{s}^{k,\star}$
 end if
 Solve the Jacobian system to compute $\delta\mathbf{s}^{k,m+1}$
 Update the saturation solution: $\mathbf{s}^{k,m+1} \leftarrow \mathbf{s}^{k,m} + \tau^{m+1} \delta\mathbf{s}^{k,m+1}$
end for

7. Numerical results

To compare the different algorithms discussed above, we consider various numerical examples with heterogeneous permeability fields. For a given time step Δt , the local phase-based CFL number is defined as

$$\text{CFL}_{\ell,K} := \frac{\Delta t \sum_{L \in \text{adj}(K)} \max(0, F_{\ell,KL}^{n+1}(\mathbf{p}^{n+1}, \mathbf{s}^{n+1}))}{V_K \phi_K}, \quad \ell = nw, w, \quad (33)$$

where V_K is the volume of the grid cell K , ϕ_K is the porosity and $F_{\ell,KL}$ is the numerical flux of the phase ℓ for the interface (KL) between cells K and L . The maximum CFL number is then computed as

$$\max \text{CFL} = \arg \max_{\ell, 1 \leq K \leq M} \text{CFL}_{\ell,K}, \quad (34)$$

where the computational domain is discretized into M cells and K is the grid cell number. In the following sections, we compare four types of solution methods for the discrete two-phase problem (8):

- FIM based on Newton’s method with damping, in which the damping parameter is chosen to ensure that the largest saturation change between two Newton iterations is smaller than 0.2. The residual is computed by discretizing (4) and using PPU to approximate the mobilities.
- The sequential fully implicit method [9–13] referred to as SFI- u_T . The outer iteration consists in two steps. We first solve the flow problem nonlinearly and compute a new total velocity field using the updated pressure. In a second step, we solve the transport problem nonlinearly with a fixed total velocity. The residual is computed by discretizing (6) and using IHU to approximate the mobilities. We have observed very slow convergence rates for SFI- p —in which the pressure is fixed during the transport solve—and we therefore do not report these results in the next sections.
- The FSMSN method of Algorithm 1. We consider two versions of the algorithm. In FSMSN- p , the transport problem is computed with a fixed pressure. The residual is computed by discretizing (4) and using PPU to approximate the mobilities. In FSMSN- u_T , the transport problem is computed with a fixed total velocity. The residual is computed by discretizing (6) and using IHU to approximate the mobilities.
- The MSPIN method of Algorithm 2 referred to as MSPIN- p . The transport problem is computed with a fixed pressure. The residual is computed by discretizing (4) and using PPU to approximate the mobilities.

7.1. SPE10 bottom layer

We first consider a horizontal test case consisting of 13,200 cells in which the porosity and permeability fields are taken from the bottom layer of the SPE10 test case [58]. We inject the wetting phase (water) from the middle well and produce from the wells located in the four corners. Capillary pressure is neglected. The phase densities are set to $\rho_w = 1025.0 \text{ kg.m}^{-3}$ and $\rho_{nw} = 849.0 \text{ kg.m}^{-3}$ and the phase viscosities are set to $\mu_w = 0.0003 \text{ Pa.s}$ and $\mu_{nw} = 0.003 \text{ Pa.s}$. We use quadratic Corey-type relative permeabilities. The domain is initially fully saturated with the non-wetting phase. We simulate 500 days of injection (0.1 total pore volume injected) with a constant time step size. The permeability and final saturation maps are shown in Fig. 1.

The nonlinear behavior of the schemes is illustrated in Fig. 2 for two selected time steps and in Table 1 for the full simulation. We consider first a fixed tolerance of 10^{-6} in the pressure and transport subproblems. We observe that for FSMSN- u_T , FSMSN- p , and MSPIN- p , the residual norm decreases at a faster rate than with Newton-based FIM and with SFI. This faster rate results in a significant reduction in the number of outer iterations. We note, however, that this reduction in the number of outer iterations requires performing a large number of subproblem iterations in FSMSN and MSPIN, which is likely to make these algorithms unpractical. For instance, FSMSN- u_T requires only 48 outer iterations—while 149 iterations are performed by Newton’s method—but involves 81 pressure iterations and 205 transport iterations.

Table 2 shows the results of the adaptive strategies introduced in Section 6 to relax the tolerance in the subproblems and reduce the computational cost of the pressure and transport steps in FSMSN and MSPIN. For both FSMSN and

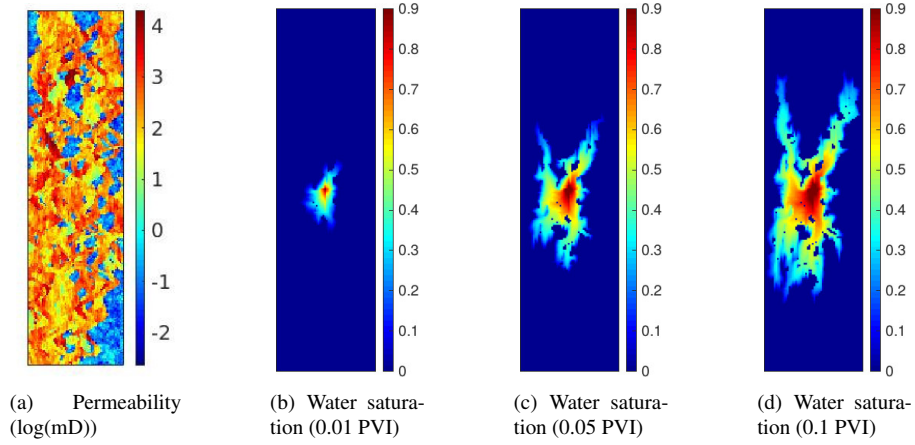


Figure 1: SPE10 bottom layer: permeability map and water saturation maps at various times.

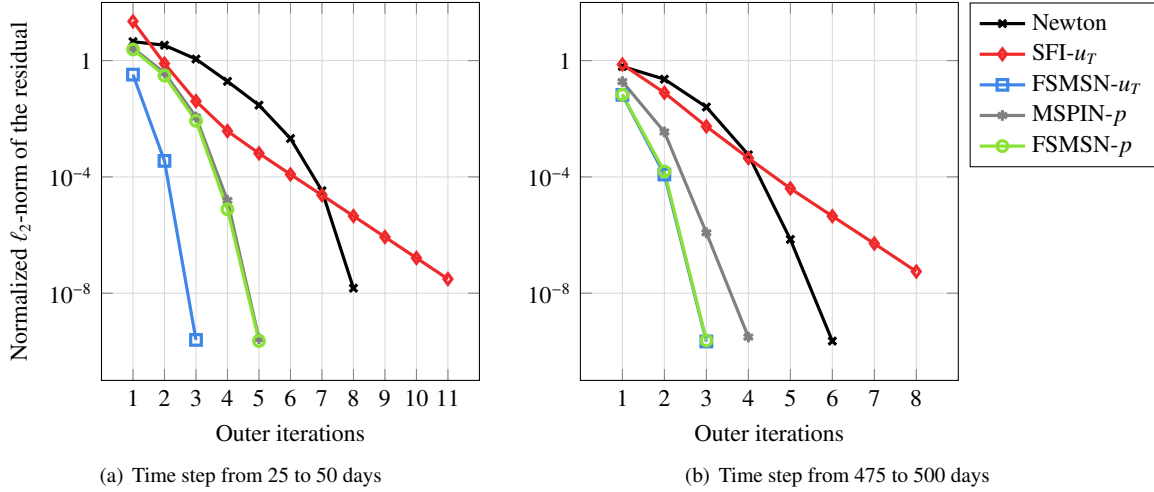


Figure 2: SPE10 bottom layer: Residual norm as a function of the number of outer iterations for two time steps. The plot on the left (respectively, on the right) corresponds to the second time step (respectively, the last time step) in the simulation. The max CFL number for these two time steps is approximately 69.

Solver	Fixed total velocity			Fixed pressure	
	Newton	SFI- u_T	FSMSN- u_T	MSPIN- p	FSMSN- p
Nonlinear iterations	149	132	48	68	56
Iterations per time step	7.5	6.6	2.4	3.4	2.8
Pressure iterations	-	204	81	116	93
Transport iterations	-	328	205	248	215

Table 1: SPE10 bottom layer: nonlinear behavior of the schemes with a fixed subproblem tolerance of 10^{-6} . The maximum CFL number is 69 and the total PVI is 0.1.

MSPIN, using adaptive tolerances in the subproblems results in a slight increase in the number of outer iterations, while the number of pressure iterations and—more significantly—the number of transport iterations are reduced.

To conclude this section, we study the sensitivity of the results to the time step size—measured by the maximum CFL number observed during the simulation. The results with a fixed tolerance and an adaptive tolerance are shown

Solver	Fixed total velocity						Fixed pressure					
	SFI- u_T			FSMSN- u_T			MSPIN- p			FSMSN- p		
	A_1	A_2	A_3	A_1	A_2	A_3	A_1	A_2	A_3	A_1	A_2	A_3
Nonlinear iterations	133	136	133	62	66	63	96	114	102	66	71	68
Iterations per time step	6.7	6.8	6.7	3.1	3.3	3.2	4.8	5.7	5.1	3.3	3.6	3.4
Pressure iterations	134	137	135	63	67	64	97	115	103	67	72	69
Transport iterations	188	178	180	109	94	107	152	150	151	110	99	110

Table 2: SPE10 bottom layer: nonlinear behavior of the schemes with an adaptive subproblem tolerance computed using the strategies (A_1), (A_2), and (A_3) of Section 6. The maximum CFL number is 69 and the total PVI is 0.1.

in Fig. 3. We observe that when the time step is increased, the number of Newton iterations is slightly reduced for CFL numbers smaller than 138, but stagnates for CFL numbers larger than 138. This is not the case for FSMSN- u_T , FSMSN- p , and MSPIN- p , as these schemes exhibit a significant reduction in the number of outer iterations as the time step is increased, even for large CFL numbers. With both fixed tolerance and adaptive tolerance in the pressure and transport subproblems, FSMSN- u_T is the solution strategy that requires the smallest number of outer iterations.

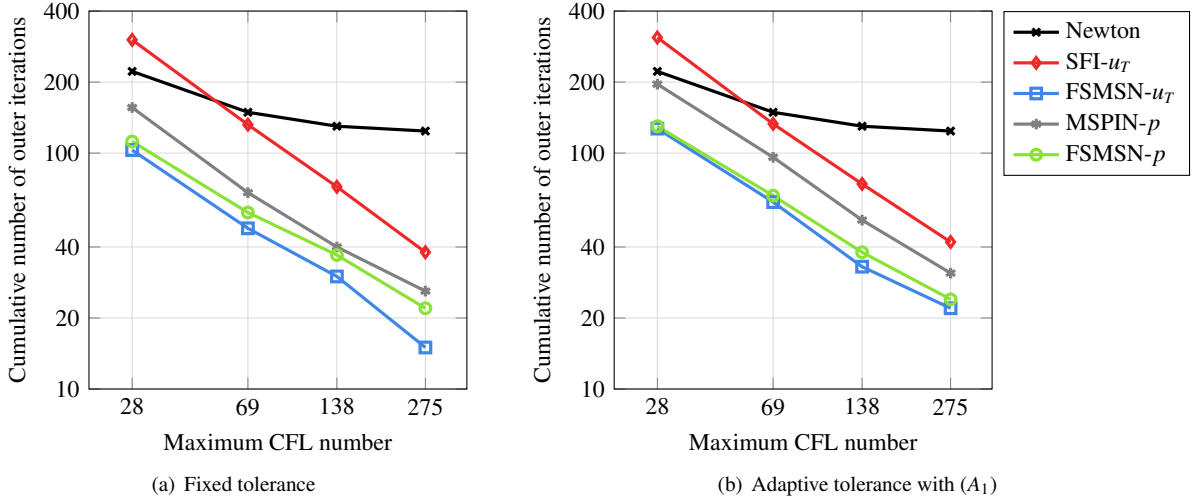


Figure 3: SPE10 bottom layer: cumulative number of outer iterations for the full simulation as a function of the maximum CFL number observed during the simulation.

7.2. SPE10 top layer

In this example, we study the impact of the introduction of buoyancy forces on the nonlinear behavior of the schemes. To do that, we consider a tilted two-dimensional domain in which the porosity and permeability fields are taken from the top layer of the SPE10 test case. The fluid properties and the well locations are the same as in the previous section. We inject 0.08 total pore volume in two distinct configurations:

- Case 1: tilting of 60° in the y -direction and fast injection rate ($9.352 \text{ m}^3/\text{day}$) so that viscous forces dominate.
- Case 2: same tilting and slower injection rate ($0.9352 \text{ m}^3/\text{day}$) so that buoyancy forces dominate.

We note that the time step size and total simulation time are adapted to obtain approximately the same maximum CFL number and total PVI in the two cases. We start the simulation with a uniform initial saturation field equal to $S_w^0 = 0$.

The nonlinear behavior of the schemes with a maximum CFL number of approximately 69 is summarized in Tables 3-4 for Case 1, and in Tables 5-6 for Case 2. We observe that increasing the strength of buoyancy forces

(relatively to viscous forces) makes the nonlinear convergence of SFI- u_T very slow, and deteriorates slightly that of MSPIN- p . However, for Newton's method, FSMSM- u_T , and FSMSN- p , we observe a slight improvement in the nonlinear behavior when buoyancy forces are stronger.

Solver	Fixed total velocity			Fixed pressure	
	Newton	SFI- u_T	FSMSN- u_T	MSPIN- p	FSMSN- p
Nonlinear iterations	135	130	51	60	56
Iterations per time step	8.43	8.12	3.19	3.75	3.5
Pressure iterations	-	496	260	314	275
Transport iterations	-	288	173	201	180

Table 3: SPE10 top layer: nonlinear behavior of the schemes with a fixed subproblem tolerance of 10^{-6} (Case 1 with fast injection rate). Approximately 2% of the interfaces experience counter-current flow. The maximum CFL number is 69 and the total PVI is 0.08.

Solver	Fixed total velocity						Fixed pressure					
	SFI- u_T			FSMSN- u_T			MSPIN- p			FSMSN- p		
	A_1	A_2	A_3	A_1	A_2	A_3	A_1	A_2	A_3	A_1	A_2	A_3
Nonlinear iterations	158	d.n.c.	164	51	56	55	80	88	89	56	58	56
Iterations per time step	9.9	d.n.c.	10.3	3.2	3.5	3.4	5	5.5	5.7	3.5	3.6	3.5
Pressure iterations	178	d.n.c.	174	69	79	69	109	114	110	74	77	73
Transport iterations	196	d.n.c.	198	85	80	90	122	115	131	90	83	96

Table 4: SPE10 top layer: nonlinear behavior of the schemes with an adaptive subproblem tolerance computed using the strategies (A_1), (A_2), and (A_3) of Section 6 (Case 1 with fast injection rate). The maximum CFL number is 69 and the total PVI is 0.08. d.n.c. denotes lack of convergence.

Solver	Fixed total velocity			Fixed pressure	
	Newton	SFI- u_T	FSMSN- u_T	MSPIN- p	FSMSN- p
Nonlinear iterations	127	567	48	67	56
Iterations per time step	7.93	33.35	3	3.18	3.5
Pressure iterations	-	1049	86	120	96
Transport iterations	-	2166	188	244	214

Table 5: SPE10 top layer: nonlinear behavior of the schemes with a fixed subproblem tolerance of 10^{-6} (Case 2 with a slower injection rate). Approximately 8% of the interfaces experience counter-current flow. The maximum CFL number is 69 and the total PVI is 0.08.

Solver	Fixed total velocity						Fixed pressure					
	SFI- u_T			FSMSN- u_T			MSPIN- p			FSMSN- p		
	A_1	A_2	A_3	A_1	A_2	A_3	A_1	A_2	A_3	A_1	A_2	A_3
Nonlinear iterations	566	d.n.c.	571	49	49	51	79	93	91	55	55	56
Iterations per time step	33.3	d.n.c.	33.6	3.1	3.1	3.2	4.9	5.8	5.7	3.4	3.4	3.5
Pressure iterations	975	d.n.c.	981	51	51	54	84	97	94	58	58	60
Transport iterations	1229	d.n.c.	1141	89	93	90	130	129	129	92	95	92

Table 6: SPE10 top layer: nonlinear behavior of the schemes with an adaptive subproblem tolerance computed using the strategies (A_1), (A_2), and (A_3) of Section 6 (Case 2 with slower injection rate). The maximum CFL number is 69 and the total PVI is 0.08. d.n.c. denotes lack of convergence.

In this section, the nonlinear behavior of FSMSN- u_T and FSMSN- p with adaptive tolerance in the subproblems remains excellent. For Cases 1 and 2, the reduction in the number of subproblem iterations obtained with the adaptive strategies is drastic but the increase in the number of outer iterations is small. However, for MSPIN- p , we observe

that using adaptive tolerances deteriorates quite significantly the nonlinear behavior, with for instance an increase by 48% in the number of outer iterations for strategy (A_3).

The sensitivity of the nonlinear behavior to the time step size is studied in Figs. 4 and 5. We note that these figures do not include the results obtained with $SFI-u_T$ as this approach does not converge for Case 2 when the CFL number is increased. As in Section 7.1, the number of Newton iterations stagnates for CFL numbers larger than 69, while the number of outer iterations required by $FSMSN-u_T$, $FSMSN-p$, and $MSPIN-p$ reduce for the range of time step sizes considered here.

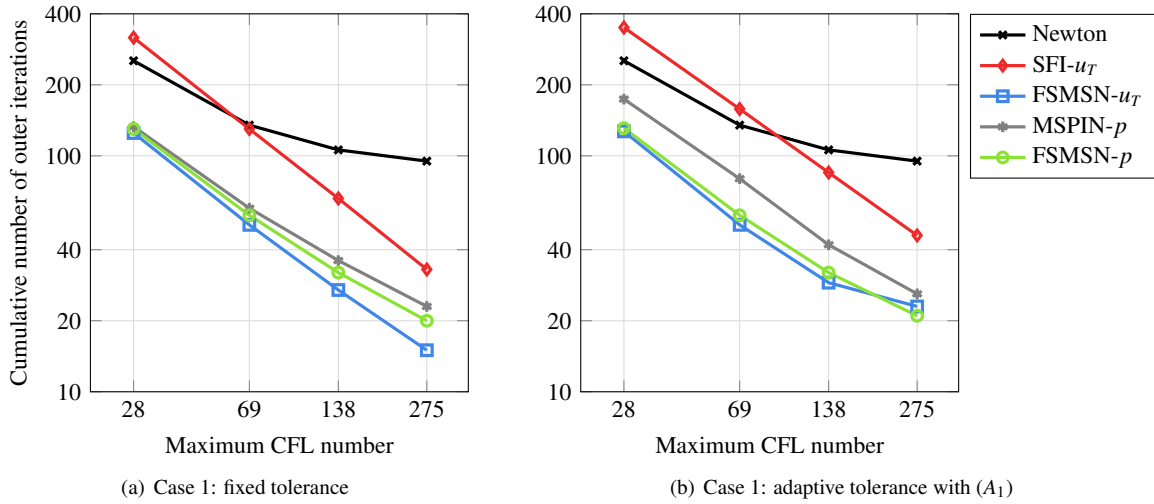


Figure 4: SPE10 top layer: cumulative number of outer iterations for the full simulation as a function of the maximum CFL number observed during the simulation (Case 1 with strong viscous forces relatively to buoyancy forces).

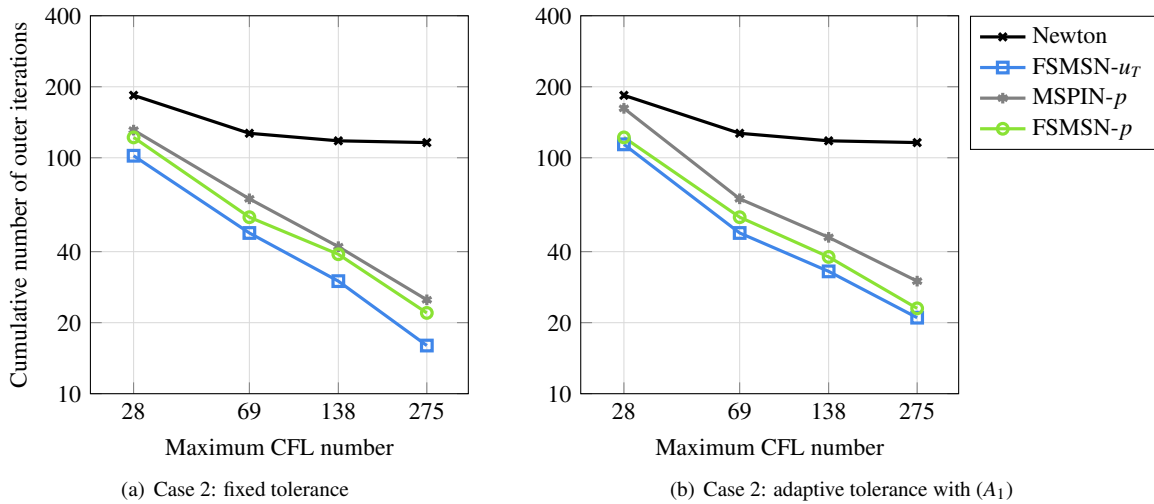


Figure 5: SPE10 top layer: cumulative number of outer iterations for the full simulation as a function of the maximum CFL number observed during the simulation (Case 2 with strong buoyancy forces relatively to viscous forces).

7.3. Gravity segregation test case

We consider a two-dimensional x - z domain of size $30.48 \text{ m} \times 30.48 \text{ m}$ divided into 100×100 cells. The domain is initially saturated with the wetting phase on the left and with the non wetting phase on the right. The phase densities and viscosities are set to $\rho_w = 1025 \text{ kg.m}^{-3}$, $\rho_{nw} = 785 \text{ kg.m}^{-3}$, $\mu_w = 0.0003 \text{ Pa.s}$, and $\mu_{nw} = 0.003 \text{ Pa.s}$. The phase relative permeabilities are quadratic. The homogeneous permeability is equal to $k = 200 \text{ mD}$. We simulate 500 days of gravity segregation with a constant time step size. The saturation maps at different times are showed in Fig. 6.

The nonlinear behavior of the schemes is summarized in Fig. 7 and in Tables 7 and 9. In this challenging buoyancy-driven test case in which flow and transport are strongly coupled, SFI requires significantly more outer iterations than FIM based on Newton's method for the case with small time steps (10 days) and fails to converge when the time step is increased. The nonlinear behavior of the solution strategies based on nonlinear preconditioning depends heavily on the formulation. Specifically, we note that nonlinear preconditioning approaches based on fixed pressure (MSPIN- p and FSMSN- p) do not perform as well as FSMSN- u_T which used a fixed total velocity to couple the flow and transport problems. Figure 7 shows that both MSPIN- p and FSMSN- p fail to converge beyond a certain time step size (10 days for MSPIN- p and 50 days for FSMSN- u_T). Importantly, FSMSN- u_T exhibits a steady reduction in the number of outer iterations as a function of time step size, which is not the case for FIM with Newton's method with which the number of iterations levels off for time step sizes larger than 50 days.

Using an adaptive tolerance in the subproblems does not alter these conclusions as shown for two different time step sizes by Tables 8 and 10. In FSMSN- u_T , the three adaptive strategies considered in this work to select the subproblem tolerance cause a slight increase in the total number of outer iterations (from 151 to 154) but achieve a large reduction in the number of subproblem iterations (from 200 to 155 for flow and from 430 to 185 for transport).

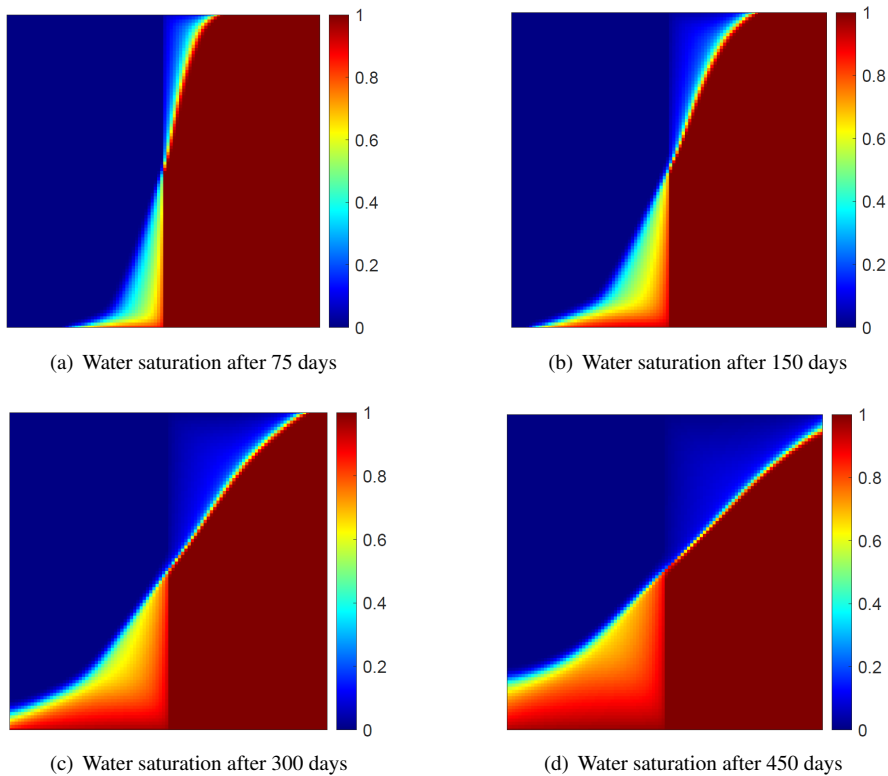


Figure 6: Gravity segregation: water saturation maps at various times.

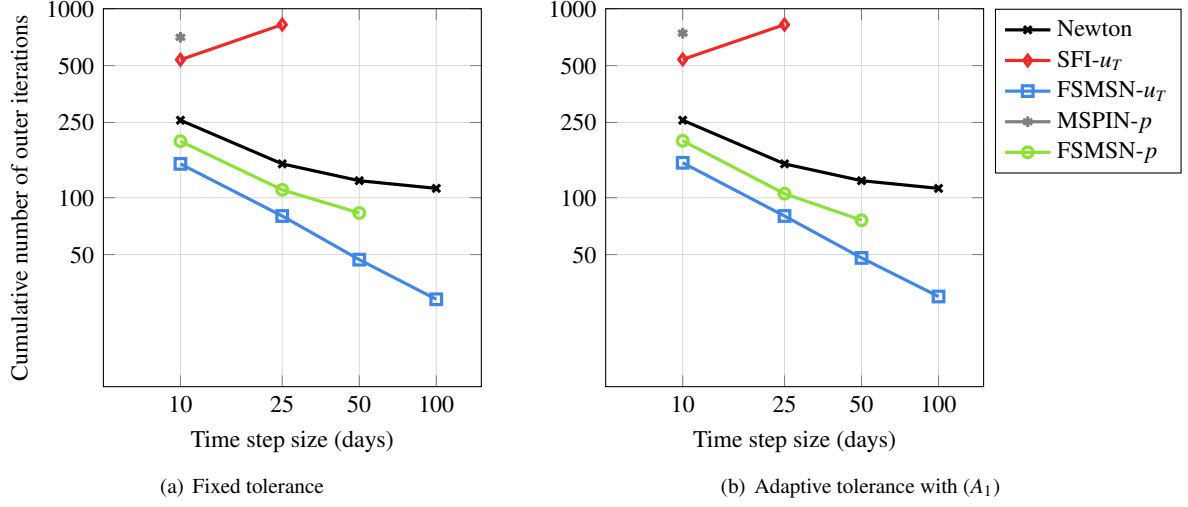


Figure 7: Gravity segregation: cumulative number of outer iterations for the full simulation as a function of time step size.

Solver	Fixed total velocity			Fixed pressure	
	Newton	SFI- u_T	FSMSN- u_T	MSPIN- p	FSMSN- p
Nonlinear iterations	257	537	151	706	199
Iterations per time step	5.14	10.74	3.02	14.12	3.98
Pressure iterations	-	678	200	852	272
Transport iterations	-	946	430	1857	642

Table 7: Gravity segregation: nonlinear behavior of the schemes with a fixed subproblem tolerance of 10^{-6} . We simulate 500 days with 50 time steps.

Solver	Fixed total velocity						Fixed pressure					
	SFI- u_T			FSMSN- u_T			MSPIN- p			FSMSN- p		
	A_1	A_2	A_3	A_1	A_2	A_3	A_1	A_2	A_3	A_1	A_2	A_3
Nonlinear iterations	539	558	558	153	154	154	743	717	712	200	200	200
Iterations per time step	10.78	11.16	11.16	3.06	3.08	3.08	14.86	14.34	14.24	4	4	4
Pressure iterations	567	580	559	155	155	155	801	1859	2909	203	201	204
Transport iterations	572	592	590	186	185	185	10761	10286	9956	262	208	218

Table 8: Gravity segregation: nonlinear behavior of the schemes with an adaptive subproblem tolerance computed using the strategies (A_1) , (A_2) , and (A_3) of Section 6. We simulate 500 days with 50 time steps.

Solver	Fixed total velocity			Fixed pressure	
	Newton	SFI- u_T	FSMSN- u_T	MSPIN- p	FSMSN- p
Nonlinear iterations	151	824	80	d.n.c.	110
Iterations per time step	7.55	41.2	4	d.n.c.	5.5
Pressure iterations	-	940	115	d.n.c.	190
Transport iterations	-	1378	265	d.n.c.	509

Table 9: Gravity segregation: nonlinear behavior of the schemes with a fixed subproblem tolerance of 10^{-6} . We simulate 500 days with 20 time steps. d.n.c. denotes lack of convergence.

Solver	Fixed total velocity						Fixed pressure					
	SFI- u_T			FSMSN- u_T			MSPIN- p			FSMSN- p		
	A_1	A_2	A_3	A_1	A_2	A_3	A_1	A_2	A_3	A_1	A_2	A_3
Nonlinear iterations	824	841	842	80	82	82	d.n.c.	d.n.c.	d.n.c.	105	105	105
Iterations per time step	41.2	42.05	42.1	4	4.1	4.1	d.n.c.	d.n.c.	d.n.c.	5.25	5.25	5.25
Pressure iterations	844	8549	845	87	83	83	d.n.c.	d.n.c.	d.n.c.	107	106	107
Transport iterations	880	8570	901	146	135	134	d.n.c.	d.n.c.	d.n.c.	247	300	231

Table 10: Gravity segregation: nonlinear behavior of the schemes with an adaptive subproblem tolerance computed using the strategies (A_1), (A_2), and (A_3) of Section 6. We simulate 500 days with 20 time steps. d.n.c. denotes lack of convergence.

7.4. Fractured heterogeneous two-dimensional model

To conclude this study, we construct a test case in which the flow is driven by competing viscous and buoyancy forces. We consider a two-dimensional x - z domain with a channelized permeability field—the channels can be seen as fractures modeled by contiguous cells with a very large permeability. The fluid properties are the same as in the previous example. The domain is initially saturated with the non-wetting phase. The wetting phase is injected through a well perforating twenty cells in the top-right part of the domain, while a producer perforates twenty cells in the bottom-left part of the domain. We simulate 1,500 days of injection (0.56 total pore volume injected). The permeability maps as well as the saturation map at different times is shown in Fig. 8

The results with fixed subproblem tolerance and adaptive tolerance are in Tables 11 and 12, respectively. The sensitivity of the nonlinear behavior of the schemes to the time step (measured by CFL number) is shown in Fig. 9. Although all the solution strategies converge well in this case, the results confirm the observations made in Sections 7.1 and 7.2. In particular, comparing the slopes of the curves for Newton-based FIM and the nonlinear preconditioners in Fig. 9 is very insightful, as it shows the improved robustness of FSMSN and MSPIN for large time step sizes.

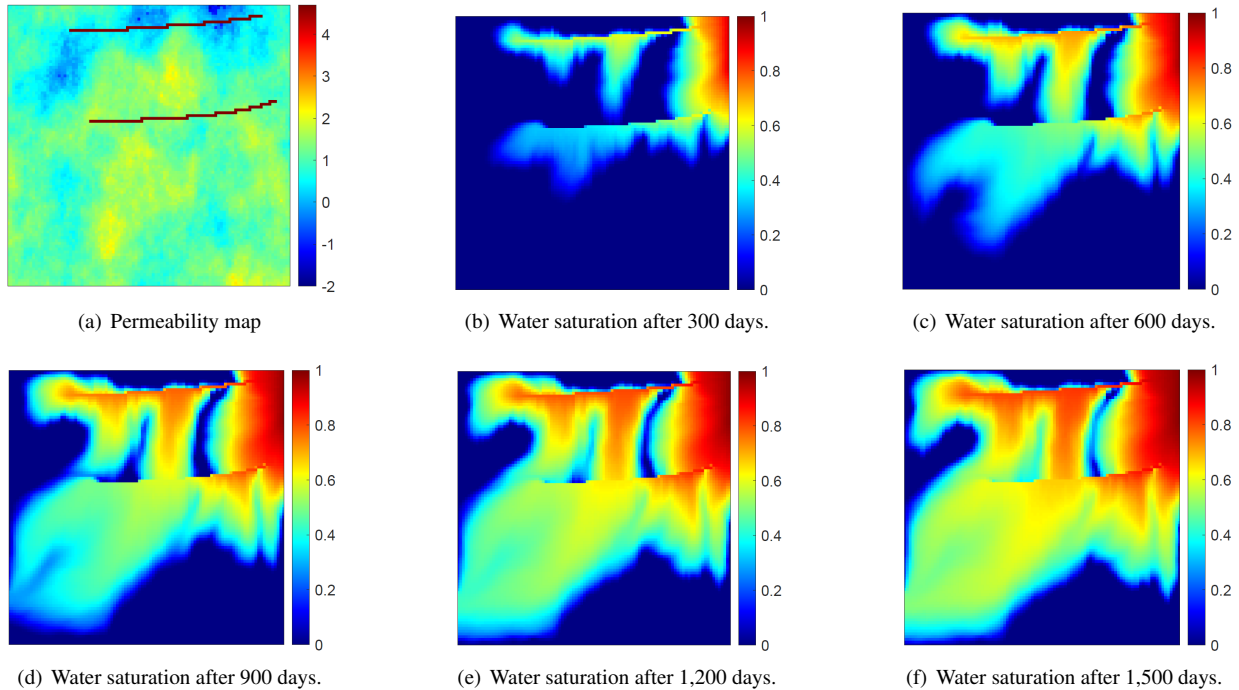


Figure 8: Permeability map of the fractured heterogeneous 2D porous media and water saturation maps at various times.

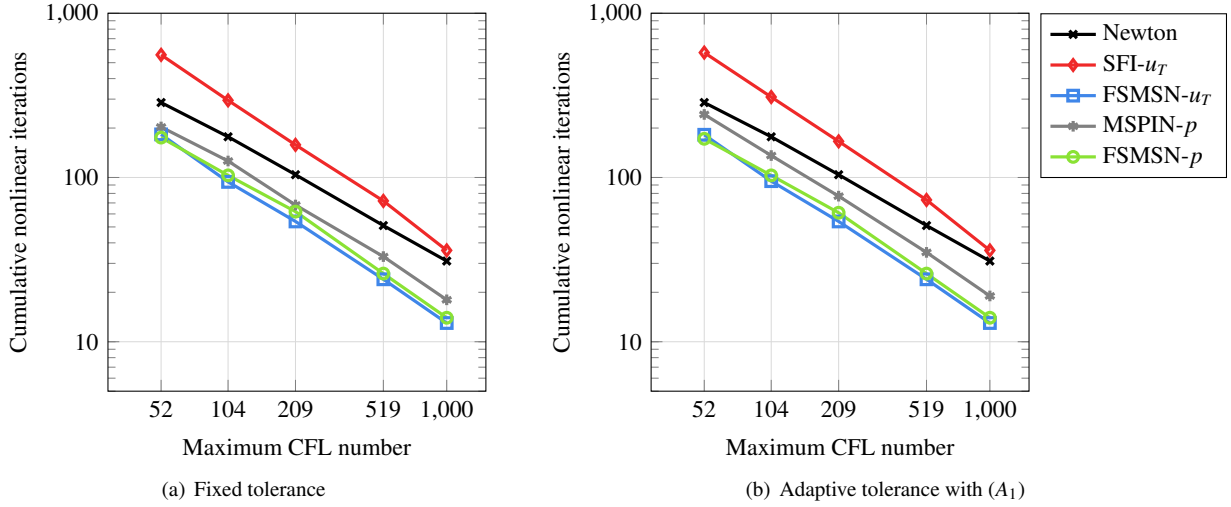


Figure 9: Fractured heterogeneous model: cumulative number of the nonlinear iterations as a function of the maximum CFL number observed during the simulation.

Solver	Fixed total velocity					Fixed pressure	
	Newton	SFI- u_T	FSMSN- u_T	MSPIN- p	FSMSN- p		
Nonlinear iterations	104	158	54	68	62		
Iterations per time step	6.93	10.53	3.6	4.53	4.13		
Pressure iterations	-	330	124	174	137		
Transport iterations	-	338	176	198	166		

Table 11: Fractured heterogeneous model: nonlinear behavior of the schemes with fixed subproblem tolerance of 10^{-6} . Approximately 2% of the interfaces experience counter-current flow. The maximum CFL number is 209 and the total PVI is 0.56.

Solver	Fixed total velocity						Fixed pressure					
	SFI- u_T			FSMSN- u_T			MSPIN- p			FSMSN- p		
	A_1	A_2	A_3	A_1	A_2	A_3	A_1	A_2	A_3	A_1	A_2	A_3
Nonlinear iterations	166	166	166	54	54	54	77	83	78	61	61	61
Pressure iterations	168	1356	168	56	56	56	82	87	83	64	64	64
Transport iterations	203	203	203	92	91	92	126	123	123	96	96	96

Table 12: Fractured heterogeneous model: nonlinear behavior of the schemes with an adaptive tolerance computed using the strategies (A_1), (A_2), and (A_3) of Section 6. The maximum CFL number is 209 and the total PVI is 0.56.

8. Conclusion

Solving the nonlinear systems that result from a fully implicit discretization of the PDEs governing multiphase flow and transport in porous media is challenging. To address this issue, we propose a field-split preconditioner referred to as Field-Split Multiplicative Schwarz Newton (FSMSN). The FSMSN-preconditioned iteration relies on two steps: a preconditioning step in which we solve sequentially a flow problem followed by a transport problem using a loose nonlinear tolerance; a global step in which we compute a Newton update for pressure and saturations by linearizing the preconditioned system. We compare its nonlinear behavior to another preconditioner of the same class (Multiplicative Schwarz Preconditioned Inexact Newton) and to standard solution strategies like Newton's method with damping to the full system, and the Sequential Fully Implicit method.

The numerical examples show that FSMSN can successfully reduce the number of outer iterations for challenging

viscous-dominated and gravity-dominated problems, compared to the other solution strategies considered here. Our results also demonstrate that this robust nonlinear behavior is preserved for large CFL numbers (corresponding to large time steps). This is key to make sure that time step sizes can be chosen based on accuracy considerations and not constrained by the nonlinear behavior of the solution strategy.

Two key steps have to be taken to show that the improved nonlinear behavior of FSMSN can result in a reduction of the computational cost of the simulation (i.e., reduction in wall-clock time). First, we plan to design a more adaptive FSMSN in which the preconditioning step would be used only when necessary, that is, for the first outer iterations of time steps with bad initial guesses and/or large sizes. As soon as the state of the system is close to the solution, the global step would be sufficient to enter the quadratic convergence regime. Second, we will substitute the direct solvers used in this work with inexact Krylov-type iterative solution strategies [56, 57, 59], which is necessary to evaluate the performance of the algorithm on large-scale problems.

Acknowledgments

Funding was provided by TotalEnergies through the FC-MAELSTROM project. The authors thank the SUPRI-B affiliates program at Stanford University and well as Joshua A. White, Nicola Castelletto (Lawrence Livermore National Laboratory), and Hervé Gross (TotalEnergies) for their insight and guidance.

References

- [1] K. Aziz, A. Settari, Petroleum reservoir simulation, Vol. 476, Applied Science Publishers London, 1979.
- [2] D. W. Peaceman, Fundamentals of Numerical Reservoir Simulation, Elsevier Scientific Publishing Company, 1977.
- [3] P. Deuffhard, Newton methods for nonlinear problems: affine invariance and adaptive algorithms, Vol. 35, Springer, 2011.
- [4] R. M. Younis, Modern advances in software and solution algorithms for reservoir simulation, Stanford University, 2011.
- [5] P. Jenny, H. A. Tchelepi, S. H. Lee, Unconditionally convergent nonlinear solver for hyperbolic conservation laws with S-shaped flux functions, *Journal of Computational Physics* 228 (20) (2009) 7497–7512.
- [6] X. Wang, H. A. Tchelepi, Trust-region based solver for nonlinear transport in heterogeneous porous media, *Journal of Computational Physics* 253 (2013) 114–137.
- [7] B. Li, H. A. Tchelepi, Nonlinear analysis of multiphase transport in porous media in the presence of viscous, buoyancy, and capillary forces, *Journal of Computational Physics* 297 (2015) 104–131.
- [8] O. Møyner, Nonlinear solver for three-phase transport problems based on approximate trust regions, *Computational Geosciences* 21 (5) (2017) 999–1021.
- [9] O. Møyner, H. A. Tchelepi, A mass-conservative sequential implicit multiscale method for isothermal equation-of-state compositional problems, *SPE Journal* 23 (6) (2018) 2376–2393.
- [10] O. Møyner, H. A. Tchelepi, A multiscale restriction-smoothed basis method for compositional models, *SPE Reservoir Simulation Conference*.
- [11] A. Moncorgé, O. Møyner, H. A. Tchelepi, P. Jenny, Consistent upwinding for sequential fully implicit multiscale compositional simulation, *Computational Geosciences* 24 (2) (2020) 533–550.
- [12] K. A. Lie, O. Møyner, J. R. Natvig, A. Kozlova, K. Bratvedt, S. Watanabe, Z. Li, Successful application of multiscale methods in a real reservoir simulator environment, *ECMOR XV - 15th European Conference on the Mathematics of Oil Recovery*.
- [13] A. Moncorgé, H. A. Tchelepi, P. Jenny, Sequential fully implicit formulation for compositional simulation using natural variables, *Journal of Computational Physics* 371 (2018) 690–711.
- [14] J. Jiang, H. A. Tchelepi, Nonlinear acceleration of sequential fully implicit (SFI) method for coupled flow and transport in porous media, *Computer Methods in Applied Mechanics and Engineering* 352 (2019) 246–275.
- [15] J. Franc, O. Møyner, H. A. Tchelepi, Coupling-strength criteria for sequential implicit formulations, *SPE Reservoir Simulation Conference*.
- [16] J. Li, P. Tomin, H. A. Tchelepi, Sequential fully implicit Newton method for compositional flow and transport, *Journal of Computational Physics* 444 (2021) 110541.
- [17] S. Watanabe, Z. Li, K. Bratvedt, S. H. Lee, J. R. Natvig, A stable multi-phase nonlinear transport solver with hybrid upwind discretization in multiscale reservoir simulator, *ECMOR XV - 15th European Conference on the Mathematics of Oil Recovery*.
- [18] R. M. Younis, H. A. Tchelepi, K. Aziz, Adaptively localized continuation-Newton method—nonlinear solvers that converge all the time, *SPE Journal* 15 (02) (2010) 526–544.
- [19] J. Jiang, H. A. Tchelepi, Dissipation-based continuation method for multiphase flow in heterogeneous porous media, *Journal of Computational Physics* 375 (2018) 307–336.
- [20] J. R. Natvig, K.-A. Lie, Fast computation of multiphase flow in porous media by implicit discontinuous Galerkin schemes with optimal ordering of elements, *Journal of Computational Physics* 227 (24) (2008) 10108–10124.
- [21] F. Kwok, H. A. Tchelepi, Potential-based reduced Newton algorithm for nonlinear multiphase flow in porous media, *Journal of Computational Physics* 227 (1) (2007) 706–727.
- [22] F. P. Hamon, H. A. Tchelepi, Ordering-based nonlinear solver for fully-implicit simulation of three-phase flow, *Computational Geosciences* 20 (5) (2016) 909–927.
- [23] Ø. S. Klemetsdal, A. F. Rasmussen, O. Møyner, K. A. Lie, Efficient reordered nonlinear Gauss-Seidel solvers with higher order for black-oil models, *Computational Geosciences* 24 (2020) 593–603.

- [24] S. Ø. Klemetsdal, O. Møyner, K. A. Lie, Robust nonlinear Newton solver with adaptive interface-localized trust regions, *SPE Journal* 24 (4) (2019) 1576–1594.
- [25] R. Toft, K.-A. Lie, O. Møyner, Full approximation scheme for reservoir simulation, *Norsk IKT-konferanse for forskning og utdanning*.
- [26] M. L. C. Christensen, P. S. Vassilevski, U. Villa, Nonlinear multigrid solvers exploiting AMGe coarse spaces with approximation properties, *Journal of Computational and Applied Mathematics* 340 (2018) 691–708.
- [27] C. S. Lee, F. P. Hamon, N. Castelletto, P. S. Vassilevski, J. A. White, Nonlinear multigrid based on local spectral coarsening for heterogeneous diffusion problems, *Computer Methods in Applied Mechanics and Engineering* 372.
- [28] C. S. Lee, F. P. Hamon, N. Castelletto, P. S. Vassilevski, J. A. White, An aggregation-based nonlinear multigrid solver for two-phase flow and transport in porous media, *Computers & Mathematics with Applications* 113 (2022) 282–299.
- [29] X.-C. Cai, D. E. Keyes, L. Marcinkowski, Non-linear additive Schwarz preconditioners and application in computational fluid dynamics, *Int. Journal for Numerical Methods in Fluids* 40 (2002) 1463–1470.
- [30] V. Dolean, M. J. Gander, W. Kheriji, F. Kwok, R. Masson, Nonlinear preconditioning: How to use a nonlinear Schwarz method to precondition Newton’s method, *SIAM Journal on Scientific Computing* 38 (0) (2016) A3357–A3380.
- [31] S. Ø. Klemetsdal, A. Moncorgé, H. M. Nilsen, O. Møyner, K. A. Lie, An adaptive sequential fully implicit domain-decomposition solver, *SPE Journal* (2021) 1–13.
- [32] O. Møyner, A. Moncorgé, Nonlinear domain decomposition scheme for sequential fully implicit formulation of compositional multiphase flow, *Computational Geosciences* 24 (2) (2020) 789–806.
- [33] S. Ø. Klemetsdal, A. Moncorgé, O. Møyner, K. A. Lie, A numerical study of the additive Schwarz preconditioned exact Newton method (ASPEN) as a nonlinear preconditioner for immiscible and compositional porous media flow, *Computational Geosciences*.
- [34] L. Luo, X.-C. Cai, D. E. Keyes, Nonlinear preconditioning for two-phase flows, *European Association of Geoscientists and Engineers*.
- [35] L. Luo, L. Liu, X.-C. Cai, D. E. Keyes, Fully implicit hybrid two-level domain decomposition algorithms for two-phase flows in porous media on 3D unstructured grids, *Journal of Computational Physics* 409.
- [36] L. Luo, X.-C. Cai, D. E. Keyes, Nonlinear preconditioning strategies for two-phase flows in porous media discretized by a fully implicit discontinuous Galerkin method, *SIAM Journal on Scientific Computing* 43 (5) (2021) S317–S344.
- [37] J. O. Skogestad, E. Keilegavlen, J. M. Nordbotten, Two-scale preconditioning for two-phase nonlinear flows in porous media, *Transport in porous media* 114 (2) (2016) 485–503.
- [38] Z. Y. Wong, F. Kwok, R. N. Horne, H. A. Tchelepi, Sequential-implicit Newton’s method for multiphysics simulation, *Journal of Computational Physics* 391 (2019) 155–178.
- [39] L. Liu, D. Keyes, Field-split preconditioned inexact Newton algorithms, *SIAM Journal on Scientific Computing* 37 (3) (2015) A1388–A1409.
- [40] P. H. Sammon, An analysis of upstream differencing, *SPE Reservoir Engineering* 3 (3) (1988) 1053–1056.
- [41] Y. Brenier, J. Jaffré, Upstream differencing for multiphase flow in reservoir simulation, *Journal on Numerical Analysis* 28 (3) (1991) 685–696.
- [42] S. H. Lee, Y. Efendiev, H. A. Tchelepi, Hybrid upwind discretization of nonlinear two-phase flow with gravity, *Advances in Water Resources* 82.
- [43] S. H. Lee, Y. Efendiev, Hybrid discretization of multi-phase flow in porous media in the presence of viscous, gravitational, and capillary forces, *Computational Geosciences* 22 (2018) 1403–1421.
- [44] F. P. Hamon, B. T. Mallison, H. A. Tchelepi, Implicit hybrid upwind scheme for coupled multiphase flow and transport with buoyancy, *Computer Methods in Applied Mechanics and Engineering* 311 (2016) 599–624.
- [45] F. P. Hamon, H. A. Tchelepi, Analysis of hybrid upwinding for fully-implicit simulation of three-phase flow with gravity, *SIAM Journal on Numerical Analysis* 54 (3) (2016) 1682–1712.
- [46] F. P. Hamon, B. T. Mallison, Fully implicit multidimensional hybrid upwind scheme for coupled flow and transport, *Computer Methods in Applied Mechanics and Engineering* 358.
- [47] S. B. M. Bosma, F. P. Hamon, B. T. Mallison, H. A. Tchelepi, Smooth implicit hybrid upwinding for compositional multiphase flow in porous media, *Computer Methods in Applied Mechanics and Engineering* 388.
- [48] K. Brenner, R. Masson, E. Quenjel, Vertex approximate gradient discretization preserving positivity for two-phase Darcy flows in heterogeneous porous media, *Journal of Computational Physics* 409.
- [49] S. Eisenstat, H. Walker, Choosing the forcing terms in an inexact Newton method, *SIAM Journal on Scientific Computing* 17 (1) (1996) 16–32.
- [50] R. Dembo, S. Eisenstat, T. Steihaug, Inexact Newton methods, *SIAM Journal on Numerical Analysis* 19 (2) (1982) 400–408.
- [51] S. Eisenstat, H. Walker, Globally convergent inexact Newton methods, *SIAM Journal on Optimization* 4 (2) (1994) 393–422.
- [52] Y. Zhou, J. Jiang, P. Tomin, Inexact methods for black-oil Sequential Fully Implicit (SFI) scheme, *SPE Reservoir Simulation Conference*.
- [53] J. Jiang, P. Tomin, Y. Zhou, Inexact methods for Sequential Fully Implicit (SFI) reservoir simulation, *Computational Geosciences* 23 (5) (2021) 1709–1730.
- [54] S. Sheth, A. Moncorgé, Inexact Newton method for general purpose reservoir simulation, *arXiv preprint arXiv:1912.06568*.
- [55] A. H. Alali, F. P. Hamon, B. T. Mallison, H. A. Tchelepi, Finite-volume simulation of capillary-dominated flow in matrix-fracture systems using interface conditions, *Computational Geosciences* 25 (1) (2021) 17–33.
- [56] Y. Saad, M. H. Schultz, GMRES: A generalized minimal residual algorithm for solving nonsymmetric linear systems, *SIAM Journal on Scientific and Statistical Computing* 7 (3) (1986) 856–869.
- [57] P. N. Brown, Y. Saad, Hybrid Krylov methods for nonlinear systems of equations, *SIAM Journal on Scientific and Statistical Computing* 11 (3) (1990) 450–481.
- [58] M. A. Christie, M. J. Blunt, Tenth SPE comparative solution project: A comparison of upscaling techniques, *Society of Petroleum Engineers*.
- [59] D. R. Fokkema, G. L. G. Sleijpen, H. A. V. der Vorst, Accelerated inexact Newton schemes for large systems of nonlinear equations, *SIAM Journal on Scientific Computing* 19 (2) (1998) 657–674.